Draelos-Hagerty, L., Paramore, J.D., Butler, B.G., Nandwana, P. and Srivastava, A., 2023. Hydrogen-Aided Microstructural Engineering of Additively Manufactured Ti–6Al–4V. Metallurgical and Materials Transactions B, 54(6), pp.3451-3461.

Hydrogen-Aided Microstructural Engineering of Additively Manufactured Ti-6Al-4V

Lara Draelos-Hagerty[1], James D. Paramore[1,2], Brady Butler[1,2], Peeyush Nandwana[3], Ankit Srivastava[1,*]

[1]Department of Materials Science & Engineering, Texas A&M University, College Station, TX 77843, USA
[2]DEVCOM Army Research Laboratory, College Station, TX 77843, USA
[3]Materials Science and Technology Division, Oak Ridge National Laboratory, Knoxville, TN 37932, USA

[*]*Corresponding Author:* ankit.sri@tamu.edu, +1 979 458 9841

ABSTRACT: Electron beam melting (EBM) additive manufacturing of Ti-6Al-4V subjects the material to complex thermal cycles, resulting in a columnar morphology of the prior β grains (PBGs). While the columnar PBGs of EBM-processed Ti-6Al-4V can be transformed to an equiaxed morphology through super-transus (i.e., above the β-transus temperature) heat-treatment, this also leads to the formation of coarse lamellar two-phase microstructure. Such a microstructure is prone to strain localization and premature fracture. Herein, we present a thermohydrogen post-process treatment that achieves equiaxed PBG morphology in EBM-processed Ti-6Al-4V without sacrificing mechanical properties. Our results show that a three-step thermohydrogen post-process treatment can transform the columnar PBG morphology to an equiaxed morphology with fine microstructure and, strength and ductility levels comparable to those of the most optimum as-fabricated samples. This three-step thermohydrogen post-process treatment involves hydrogenation and phase transformation treatment in a hydrogen atmosphere, and subsequent dehydrogenation treatment in vacuum. Notably, all these treatments are carried out at temperatures well below the β-transus temperature of hydrogen-free Ti-6Al-4V.

KEYWORDS: Characterization; Tensile testing; Additive manufacturing; Titanium alloys; Phase transformation; Hydrogen processing

I. INTRODUCTION

Layer-by-layer additive manufacturing, such as electron beam melting (EBM, also known as electron beam powder bed fusion), of Ti-6Al-4V produces unique, process specific microstructures[1-3]. Specifically, during EBM, the large thermal gradients and complex thermal cycling, which involves preheating, melting, rapid cooling, and partial re-melting of each layer, results in columnar prior β grains (PBGs) along the build direction with a $\langle 001 \rangle$ fiber texture[4-8]. This columnar grain morphology in EBM-processed Ti-6Al-4V as well as in other additive manufacturing processes, such as laser powder bed fusion (LPBF) and directed energy deposition (DED)[9-10] is in contrast to the conventional manufacturing processes (e.g., wrought processing) that leads to equiaxed grain morphologies[11]. The columnar microstructure produced during additive manufacturing renders the material mechanically anisotropic, which can adversely affect the mechanical performance. For example, latitudinally oriented tensile specimens (i.e., the tensile axis normal to the build direction) generally exhibit lower tensile strengths for both EBM- and LPBF-processed materials compared to longitudinally orientated tensile specimens (i.e., tensile axis parallel to the build direction)[12-13]. Similarly, latitudinally oriented specimens exhibit inferior resistance to fatigue compared to the longitudinally oriented specimens[14]. Thus, the anisotropic microstructure as well as other process-induced defects (e.g., lack of fusion and keyhole porosity[3]) predispose additively manufactured Ti-6Al-4V to premature failure[15-17].

To reduce the process-induced defects, additively manufactured materials are typically subjected to post-process hot isostatic pressing (HIP) treatments[18]. During HIP, the pressure at high temperature aids in pore closure, while the associated heat-treatment impacts the microstructure[18]. It has been shown that a single-stage heat-treatment below the β-transus temperature (i.e., sub-transus) only coarsens the as-fabricated α-phase microstructure, which does not affect the anisotropy but leads to a decrease in the as-fabricated strength[19-20]. Recently it has been shown that a three-stage sub-transus heat-treatment can improve the mechanical properties of LPBF deposited Ti-6Al-4V but it still maintains the columnar PBG morphology[21]. On the other hand, heat-treatment above the β-transus temperature (i.e., super-transus) transforms the columnar PBG morphology to an equiaxed morphology and eliminates

macroscopic anisotropy[7, 12, 20]. Although the super-transus heat-treatment leads to an equiaxed PBG morphology with strength levels that can be greater than the sub-transus heat-treatment, it also transforms the α-phase morphology from basketweave to lamellar[7, 12, 20]. The Ti-6Al-4V microstructures with lamellar α-phase are prone to strain localization and result in relatively lower ductility[20]. More importantly, even though there has been some success in obtaining equiaxed-like PBG morphology by optimizing scanning strategies of LPBF process[22] or reducing thickness of the columnar PBGs by introducing heat sinks in EBM process[23]; it is not easy to directly process Ti-6Al-4V with equiaxed PBGs and fine α-phase microstructure using all current additive manufacturing techniques due to their limited constitutional supercooling[24]. Therefore, a post-process super-transus heat-treatment is necessary to form an equiaxed microstructure in additively manufactured Ti-6Al-4V. This leads to a fundamental question of technological relevance: how can the columnar PBG morphology of additively manufactured Ti-6Al-4V be engineered to an equiaxed morphology without sacrificing the mechanical properties?

To this end, we explore the viability of thermohydrogen post-process treatments to achieve equiaxed PBG morphologies in EBM-processed Ti-6Al-4V while simultaneously maintaining the strength and ductility levels of the optimally oriented as-fabricated material. Thermohydrogen treatments involve subjecting a material to heat-treatments in a hydrogen atmosphere. Similar processing has been previously applied to Ti-6Al-4V fabricated via wrought processing[25-29], powder metallurgy[30-31], and LPBF additive manufacturing routes[32]. These works have shown that thermohydrogen treatments of Ti-6Al-4V can transform a variety of initial microstructure types, such as lamellar, Widmanstätten, bi-modal, and even relatively coarse equiaxed, to a fine equiaxed morphology without any mechanical deformation. During thermohydrogen treatments, hydrogen works as a temporary alloying element in Ti-6Al-4V and enables phase transformations that are not otherwise possible[25, 28]. As a β stabilizer in titanium alloys, hydrogen lowers the β-transus temperature. Furthermore, the presence of hydrogen allows for homogeneous precipitation of low temperature phases, producing ultrafine α grains that can be engineered into a wide range of microstructures without requiring deformation-based processing[29-32]. Specifically, Paramore et al.[30-31] proposed a five-step thermohydrogen treatment procedure for powder metallurgy processing of Ti-6Al-4V that yielded wrought-like microstructures and mechanical properties. The five-step thermohydrogen treatment in those

works involved sintering, phase transformation, dehydrogenation, globularization, and aging steps.

Herein, we modify the five-step thermohydrogen treatment proposed by Paramore et al.[30-31] to achieve an equiaxed PBG morphology in EBM-processed Ti-6Al-4V. We show that a reduced three-step thermohydrogen post-process treatment is sufficient to transform the as-fabricated PBG morphology from columnar to equiaxed, while producing a fine α-phase microstructure. This three-step thermohydrogen post-process treatment involves hydrogenation, phase transformation, and dehydrogenation steps, wherein all treatments are carried out at temperatures well below the β-transus temperature of hydrogen-free Ti-6Al-4V. The resulting mechanical properties, such as strength and ductility, of the three-step thermohydrogen treated EBM-processed Ti-6Al-4V samples are on par with the strength and ductility levels of optimally oriented as-fabricated samples. This is in contrast to existing heat-treatments, which often lead to reductions in either strength, ductility, or both as compared to the as-fabricated condition for EBM-processed materials.

The ability to engineer equiaxed PBG morphology in Ti-6Al-4V samples using thermohydrogen treatment is of particular importance for additive manufacturing. Traditional methods, which rely on thermomechanical processing to achieve such microstructure, are not viable for additively manufactured samples as they undermine the intrinsic benefit of additive manufacturing, which is the production of near-net-shaped components. Moreover, the decrease in the β-transus temperature via hydrogenation is crucial, as a lower β-transus temperature facilitates the emergence of finer α-phase laths, which are essential for high strength. This is primarily due to the slower growth kinetics of the α-phase at lower $\beta \rightarrow \alpha$ transformation temperatures. Importantly, the combination of decreased temperature requirements and the elimination of deformation-based processing substantially reduces energy costs and makes this methodology particularly well-suited for optimizing the microstructure of EBM-processed Ti-6Al-4V.

II. METHODS

A. *Material fabrication*

Ti-6Al-4V material considered in this work was fabricated using an Arcam Q10 EBM system and standard Arcam processing parameters at the Powder Metals & Additive Manufacturing Facility of Oak Ridge National Laboratories. The material was fabricated as cylinders of diameter 0.58" and length 4" using pre-alloyed atomized Ti-6Al-4V powders supplied by Advanced Powders and Coating (AP&C, Quebec, Canada). The powders had a nominal composition of 5.28wt% Al, 4.23wt% V, 0.14wt% O, 0.20wt% Fe and the remainder Ti. The nominal hydrogen content of the powders is extremely low (on the order of 0.0001wt%). More details of the EBM process used in this study can be found in refs.[12, 19, 33].

B. *Post-process treatments*

The EBM-processed Ti-6Al-4V cylindrical samples were subjected to six sets of post-process treatments. The nomenclature and description of all six post-process treatments are given in Table I. For the hydrogen atmosphere, a 50/50 mixture of H_2 and Ar gas was used, with both gases simultaneously maintained at a flow rate of 1L/min using Aalborg GFC-17 mass flow controllers, while the (near) vacuum atmosphere was achieved by maintaining an absolute pressure below 1×10^{-5}torr. The heating and cooling rates for all post-process heat-treatments were approximately 10ºC/min.

The first two sets of post-process treatments, V850 and V1025, served as controls to assess the effect of the thermal profile (as shown schematically in Fig. 1) in the absence of a hydrogen-containing atmosphere. Therefore, all five-steps of the post-process treatments were carried out in vacuum. Step I of this five steps of these post-process treatment were carried out at a temperature/time combination of 850°C/1h for V850 and 1025°C/1h for V1025. For both V850 and V1025, steps II-V were carried out at temperature/time combinations of 650°C/4h, 750°C/12h, 950°C/1h, and 550°C/6h, respectively. It must be noted that in a hydrogen-free

atmosphere, 1025°C is above the β-transus temperature for Ti-6Al-4V while 850°C is below the β-transus temperature.

Table I. Nomenclature and description of the various post-process treatments carried out in this work.

Nomenclature	*Post-process treatments*
V850	Vacuum atmosphere: 850°C/1hr, 650°C/4h, 750°C/12h, 950°C/1hr, 550°C/6h
V1025	Vacuum atmosphere: 1025°C/1hr, 650°C/4h, 750°C/12h, 950°C/1hr, 550°C/6h
5H850	Hydrogen atmosphere: 850°C/1hr, 650°C/4h Vacuum atmosphere: 750°C/12h, 950°C/1hr, 550°C/6h
5H1025	Hydrogen atmosphere: 1025°C/1hr, 650°C/4h Vacuum atmosphere: 750°C/12h, 950°C/1hr, 550°C/6h
3H850	Hydrogen atmosphere: 850°C/1hr, 650°C/4h Vacuum atmosphere: 750°C/12h
3H1025	Hydrogen atmosphere: 1025°C/1hr, 650°C/4h Vacuum atmosphere: 750°C/12h

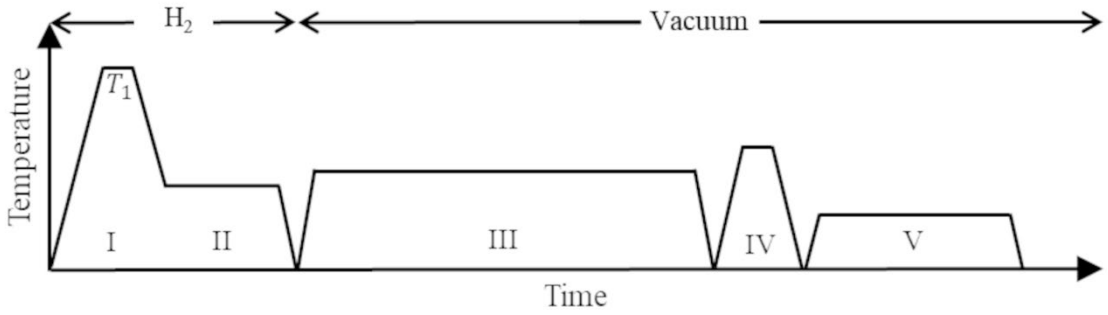

Fig. 1 – A schematic representation of all the steps involved in the post-process thermohydrogen treatment. The steps I-V correspond to hydrogenation, phase transformation, dehydrogenation, globularization and aging, respectively.

The second two sets of the post-process treatments, 5H850 and 5H1025, involved subjecting the samples to the full five-step thermohydrogen treatment proposed by Paramore et al.[30-31] and shown schematically in Fig. 1. The five-steps involved in this treatment are, hydrogenation (I), phase transformation (II), dehydrogenation (III), globularization (IV) and aging (V). The first two steps of this five-step treatment were carried out in the hydrogen atmosphere and the last three steps were carried out in vacuum condition. For 5H850, the hydrogenation temperature (T_1) was maintained at 850°C, while for 5H1025, T_1 was 1025°C. The hydrogenation step (I) for both post-process treatments were carried out for 1h. Also, for both 5H850 and 5H1025, the phase transformation, dehydrogenation, globularization and aging steps were carried out at temperature/time combinations of 650°C/4h, 750°C/12h, 950°C/1h, and 550°C/6h, respectively.

The last two sets, 3H850 and 3H1025, of the post-process treatments aimed at separating the effects of the first three steps of the five-step post-process thermohydrogen treatment. Thus, these samples were only subjected to the first three steps shown in Fig. 1. Step I of the three-step post-process thermohydrogen treatment was carried out at a temperature/time combination of 850°C/1h for 3H850 and 1025°C/1h for 3H1025. For both 3H850 and 3H1025, steps II and III were carried out at temperature/time combinations of 650°C/4h and 750°C/12h, respectively.

C. *Hydrogen quantification*

The hydrogen content in the as-fabricated as well as in all post-processed Ti-6Al-4V samples were quantified using a high-performance O, N and H analyzer (G8 Galileo, Bruker Corporation) and following the ASTM E1447-09 standard[34]. The G8 Galileo works on the principle of inert gas fusion via melt extraction. In this process, the material is melted in a graphite crucible, and hydrogen is evolved from the material as H_2 gas and swept by the carrier gas (N_2) through a thermal conductivity cell to determine the amount of hydrogen in the gas stream. Nitrides will form on the surface of Ti alloys when using N_2 carrier gas, preventing the release of H_2. Therefore, Bruker recommends the inclusion of high-purity Sn pellets to coat the samples and prevent the formation of surface nitrides, which was done with all the specimens in this study.

D. *Tensile testing*

Cylindrical dog-bone tensile specimens with 6.35mm diameter and 25.4mm gauge length of both as-fabricated and all post-process treated Ti-6Al-4V samples were machined following the ASTM E8/E8M standard[35] and mechanically tested under uniaxial tensile loading conditions. At least one additional tensile test specimen was machined and tested for each sample type, both as-fabricated and all post-processed, to ascertain the reproducibility of the measured mechanical properties of the samples. All uniaxial tensile tests were carried out using a servo-hydraulic load frame (MTS) equipped with a 50kN load cell and at ambient conditions at an imposed displacement rate of 0.0125mm/s giving a nominal strain rate of $0.5 \times 10^{-3} s^{-1}$. The extension in the gauge section of all the tensile specimens were measured using a 25.4mm extensometer.

E. *Microstructure and fracture surface characterization*

The metallographic specimens of both as-fabricated and all post-processed samples were mechanically polished following a procedure that involved wet grinding using ANSI 320 SiC paper followed by rough polishing using 9μm diamond paste on a napless cloth for 10mins, and fine polish using a mixture of 1 part 30% H_2O_2 combined with 3 parts 0.02μm colloidal silica suspension on a final polishing cloth for 10 min. Each step was finished with a 5mins sonication in ethanol. If scratches were present on the polished samples, they were re-polished using 3μm diamond paste on a napless cloth. This was again followed by a fine polish using the mixture composed of 1 part 30% H_2O_2 and 3 parts 0.02μm colloidal silica suspension on a final polishing cloth. The polishing step using the mixture of 1 part 30% H_2O_2 and 3 parts 0.02μm colloidal silica suspension is crucial for achieving a high-quality polished finish on titanium alloys. The polished metallographic specimens were imaged using the backscattered electron (BSE) imaging mode in a Tescan FERA-3 scanning electron microscope (SEM). The unpolished fracture surfaces of all the fractured tensile specimens were also analyzed using the secondary electron (SE) SEM imaging.

III. RESULTS

The hydrogen content in both as-fabricated and all post-processed conditions (defined in Table I) is given in section III.A, the microstructure and mechanical properties of all the samples are described in sections III.B and III.C, respectively, and fracture surface morphology of all the samples are presented in section III.D.

A. *Hydrogen content*

The hydrogen content in the as-fabricated and all post-processed samples are given in Table II. In all the samples, the hydrogen content is well below that of the ASTM standard requirement for Ti-6Al-4V, which is 150 ppm for grade 5 and 125 ppm for grade 23[36]. In general, the residual hydrogen content as well as their standard deviation in the samples hydrogenated at a temperature of 1025°C (step I) is greater than the samples hydrogenated at a temperature of 850°C following an otherwise similar procedure. However, being that all conditions were an order of magnitude below the ASTM specification for hydrogen content and there is no clear physical explanation for the discrepancy, this finding is likely of little importance.

Table II. The average values $\pm$ one standard deviation of the final hydrogen content (in ppm) in as-fabricated and all post-process treated Ti-6Al-4V samples.

As-fabricated	**V850**	**V1025**	**5H850**	**5H1025**	**3H850**	**3H1025**
4.7±1.9	6.2±0.9	7.5±1.0	5.9±0.5	15.1±5.4	2.4±0.2	4.8±1.6

B. *Material microstructure*

Relatively low-magnification, panoramic BSE-SEM images of the microstructure of as-fabricated and all six post-processed conditions are shown in Fig. 2. Also, representative high magnification BSE-SEM images of the microstructures of all these conditions are shown in Fig. 3. In all the BSE-SEM images, the light-contrast phase is the vanadium-rich β-phase while the darker-contrast phase is the aluminum-rich α-phase. Multiple BSE-SEM images of the microstructures of all the conditions were also used to quantify sizes of all relevant features in

the microstructures using a method analogous to the line intercept method (originally developed to measure grain sizes as outlined in ASTM E112-13[37]), and are given in Table III.

Table III. The average values ± one standard deviation of sizes of all relevant features in the microstructures of as-fabricated and all post-process treated Ti-6Al-4V samples.

	Prior β grains	**α colonies**	**α laths**	**Grain boundary α**
As-fabricated	162.5±55.7μm*	-	0.8±0.2μm	2.5±1.1μm
V850	161.9±56.6μm*	-	3.2±0.8μm	5.4±0.9μm
V1025	616.8±169.0μm	285±89μm	5.2±1.1μm	8.4±1.7μm
5H850	536.0±159.6m	-	3.8±1.3μm	8.0±1.5μm
5H1025	713.2±127.9μm	-	4.1±0.9μm	8.0±1.7μm
3H850	353.4±115.8μm	-	1.3±0.3μm	2.5±0.6μm
3H1025	462.6±165.7μm	-	1.3±0.5μm	4.0±1.6μm
*Quantities reported are the width of the prior β grains; the length (dimension along the build direction) of the grains is approximately over 1mm.				

As shown in Figs. 2(a) and 3(a), the microstructure of the as-fabricated samples comprises columnar PBGs. Within the PBGs are ribs of retained β-phase that separate fine α-phase laths, producing a basketweave morphology. This microstructure is typical of EBM-processed Ti-6Al-4V samples. The five-step heat-treatment of the as-fabricated samples in vacuum at T_1 = 850ºC which is below the β-transus temperature, mainly led to coarsening of the as-fabricated α-phase laths while maintaining the columnar PBG and basketweave α morphology, as shown in Figs. 2(b) and 3(b) for V850 condition. The sizes of all relevant features in the microstructures of as-fabricated and V850 samples are compared in Table III.

A five-step heat-treatment of the as-fabricated samples in vacuum at T_1=1025ºC which is above the β-transus temperature, resulted in the transformation of the initial columnar PBG morphology to an equiaxed morphology, as shown in Fig. 2(c) for V1025 sample. The transformation of the PBG morphology in V1025 sample was also accompanied by the transformation of the α-phase morphology from basketweave to coarse lamellar as well as formation of relatively coarse grain boundary α (i.e., continuous α-phase along the PBG

boundaries), as can be seen in the higher magnification image in Fig. 3(c). The sizes of all relevant features in the microstructure of V1025 samples are given in Table III.

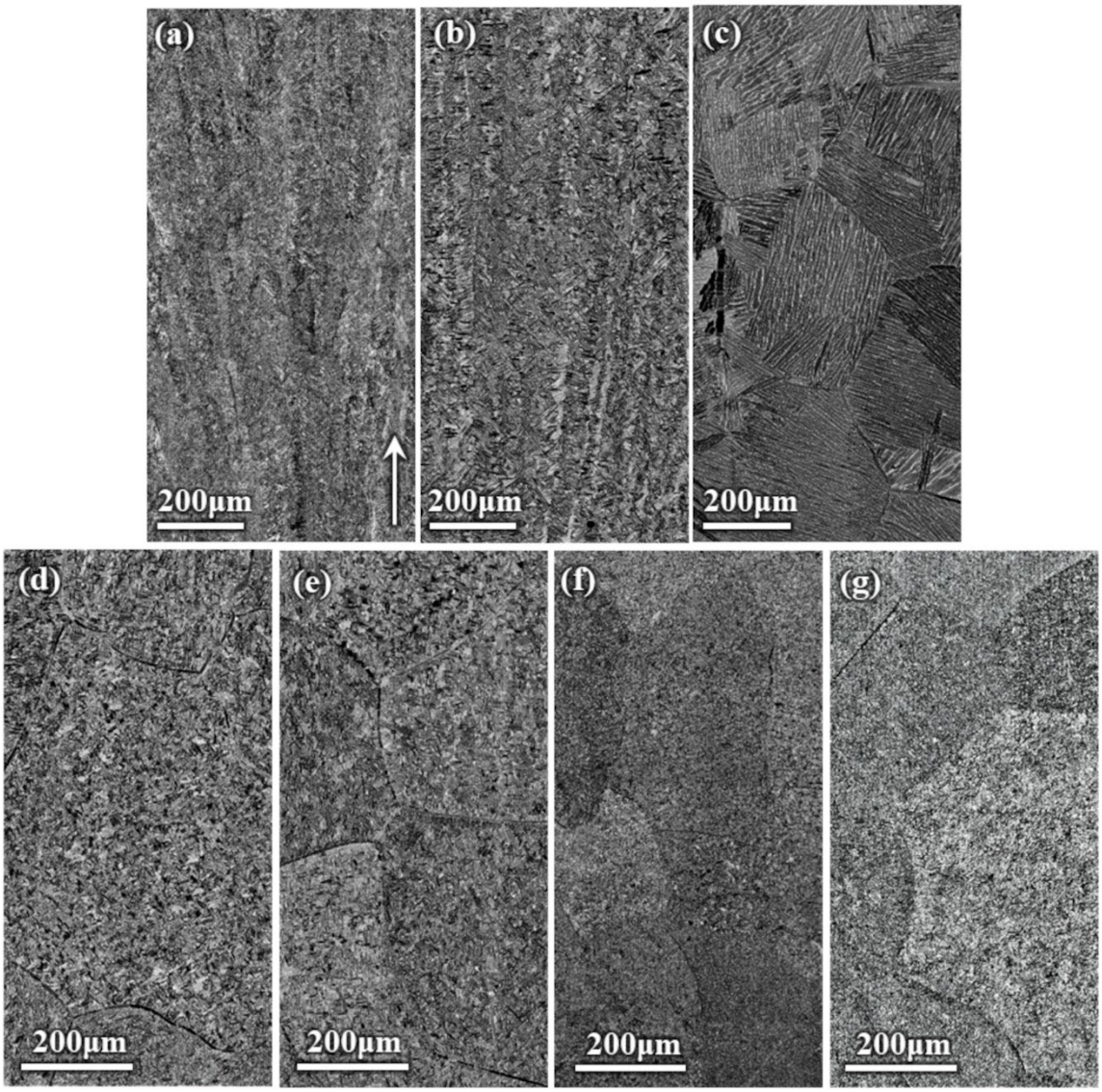

Fig. 2 – Panoramic BSE-SEM images of the microstructure of (a) as-fabricated, (b) V850, (c) V1025, (d) 5H850, (e) 5H1025, (f) 3H850, and (g) 3H1025 samples. The build direction of the EBM-processed material is marked with an arrow in (a) and is same in (b)-(g). The scale-bar shown in (a) is the same in (b)-(g). In the images, the dark phase is α and the light phase is β. A detailed description of all the post-process treatments performed is given in Table I.

The five-step thermohydrogen treatment of the as-fabricated samples with T_1 = 850°C and 1025ºC (i.e., 5H850 and 5H1025), also resulted in equiaxed PBGs with continuous grain

boundary α, as in V1025 samples (Fig. 2). However, unlike the lamellar α-phase morphology in V1025 samples, these prior-β grains contain globularized α-phase surrounded by β-phase ribs as seen in the BSE-SEM images in Figs. 2(d) and 3(d) for 5H850 samples and Figs. 2(e) and 3(e) for 5H1025 samples. The main difference between 5H850 and 5H1025 samples is that the thermohydrogen treatment at higher hydrogenation temperature increased the PBG size. The sizes of all relevant features in the microstructures of 5H850 and 5H1025 samples are compared in Table III.

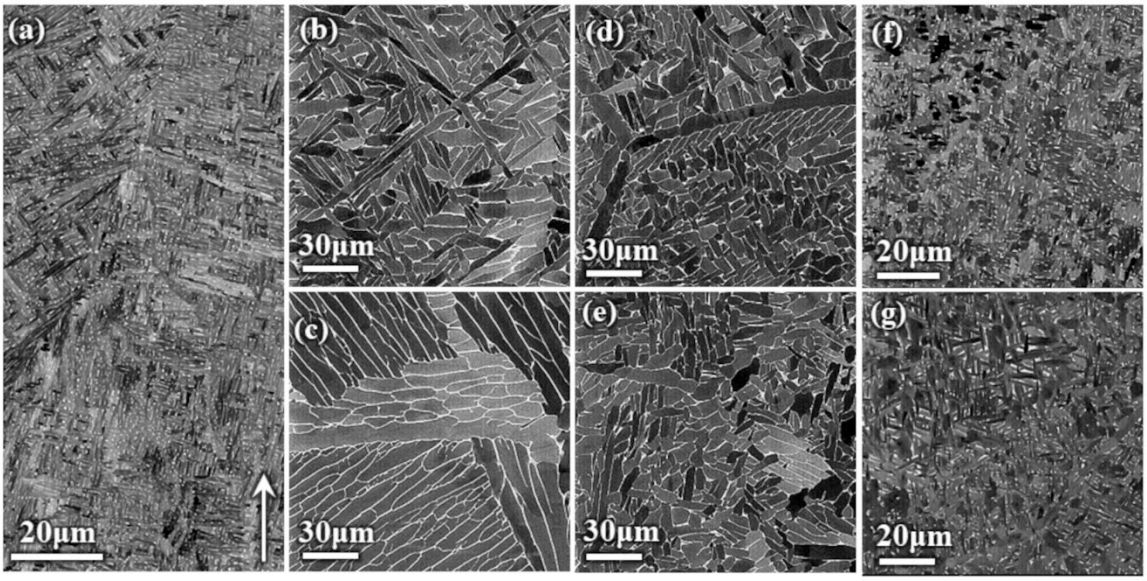

Fig. 3 – High magnification BSE-SEM images of the microstructure of (a) as-fabricated, (b) V850, (c) V1025, (d) 5H850, (e) 5H1025, (f) 3H850, and (g) 3H1025 samples. The build direction of the EBM-processed material is marked with an arrow in (a) and is same in (b)-(g). In the images, the dark phase is α and the light phase is β. A detailed description of all the post-process treatments performed is given in Table I.

The BSE-SEM images of the microstructures of the samples subjected to a reduced three-step thermohydrogen treatment are shown in Figs. 2(f) and 3(f) for 3H850 samples and Figs. 2(g) and 3(g) for 3H1025 samples. Like V1025, 5H850 and 5H1025 samples, these microstructures also contain equiaxed PBGs with continuous grain boundary α. However, the PBG in 3H850 and 3H1025 samples contain ultrafine α surrounded by discontinuous β phase. Also, as in the five-step thermohydrogen treatment process, three-step thermohydrogen treatment at higher

hydrogenation temperature resulted in larger PBGs. The sizes of all relevant features in the microstructures of 3H850 and 3H1025 samples are compared in Table III.

C. *Uniaxial tensile response*

Representative engineering tensile stress-strain curves for as-fabricated, V850, and V1025 samples are shown in Fig. 4(a) and those for 5H850, 5H1025, 3H850, and 3H1025 are shown in Fig. 4(b). The mechanical properties such as yield strength, ultimate tensile strength, and elongation obtained from the stress-strain curves in Fig. 4 as well as the reduction in area estimated from the fractured specimens are shown in Fig. 5 for all conditions. To measure the reduction in area, the minimum cross-section of the fractured specimens was measured using a Vernier caliper. This value was then subtracted from the initial nominal cross-section area of the cylindrical dog-bone specimen.

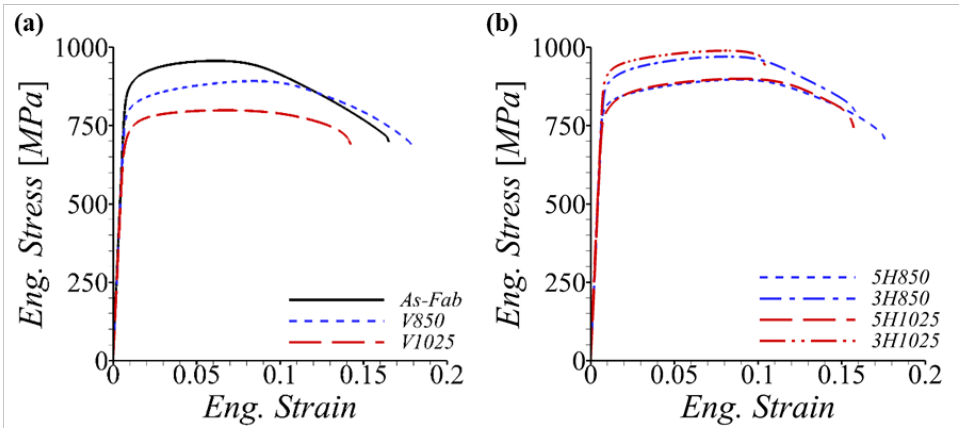

Fig. 4 – Representative engineering (Eng.) tensile stress-strain curves of (a) as-fabricated (As-Fab), V850 and V1025 samples, and those of (b) 5H850, 5H1025, 3H850 and 3H1025 samples. A detailed description of all post-process treatments performed is given in Table I.

As can be inferred from Fig. 4, all conditions exhibited rather low but appreciable work-hardening up until the ultimate tensile strength was reached, at which point necking ensued. Post-necking and before final fracture, the as-fabricated and all the samples treated at a temperature of 850°C underwent a significant amount of tensile deformation with monotonically

decreasing load carrying capacity. However, except for the 5H1025, the other two samples hydrogenated at 1025°C exhibited a small degree of post-necking deformation.

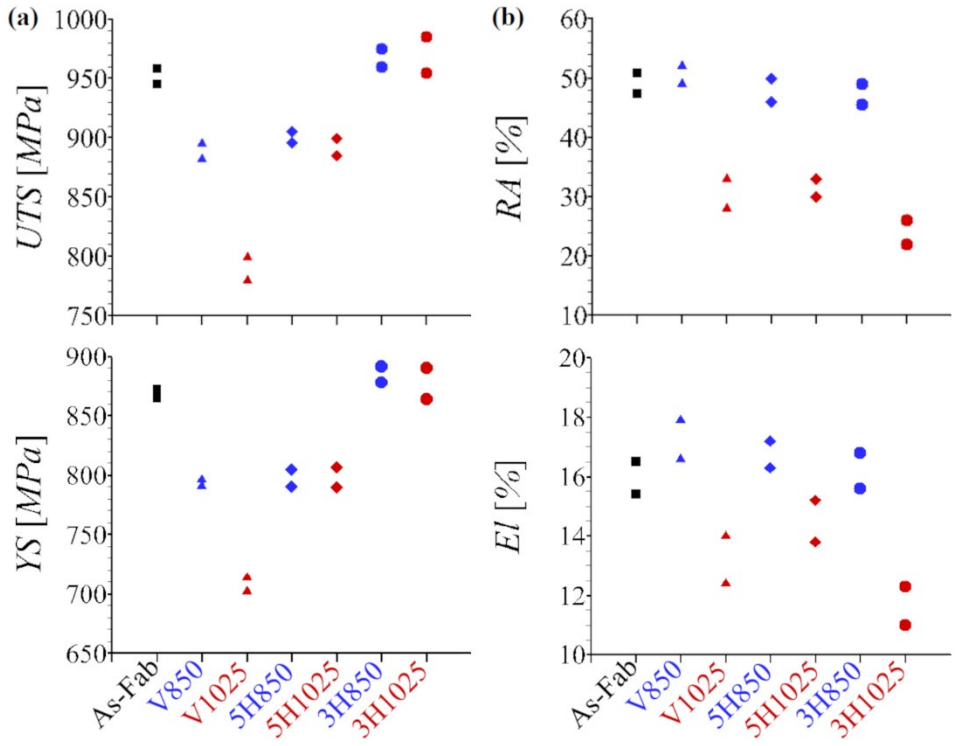

Fig. 5 – The (a) ultimate tensile strength (UTS) and yield strength (YS), and (b) percentage reduction in area (%RA) and percentage elongation (%El) of both as-fabricated and all post-process treated Ti-6Al-4V samples. A detailed description of all post-process treatments performed is given in Table I.

The vacuum heat-treatments (i.e., V850 and V1025) resulted in a decrease in the yield and ultimate tensile strengths of the material as compared to the as-fabricated material, Fig. 5(a). The decrease in the strength was greater for the V1025 samples compared to the V850 samples. Similarly, the five-step thermohydrogen treatments at T_1=850°C and 1025ºC (i.e., 5H850 and 5H1025), also resulted in a decrease in the yield and ultimate tensile strengths as compared to the as-fabricated material. Furthermore, the strength levels of the 5H850 and 5H1025 samples are comparable to that of the V850 samples. The reduced three-step thermohydrogen treatment (i.e., 3H850 and 3H1025), did not result in any appreciable change in the yield and ultimate tensile

strengths as compared to the as-fabricated material despite the large differences in the microstructures.

As can be seen in Fig. 5(b), the percentage elongation and the percentage reduction in area are roughly the same for the as-fabricated and all treatments (vacuum or thermohydrogen) done at T_1=850°C. However, the ductility of the samples subjected to vacuum or thermohydrogen treatments at T_1=1025°C are lower than that of the as-fabricated samples, with the ductility values being lowest for the 3H1025 condition.

D. *Fracture surface morphology*

Representative SE-SEM images of fracture surfaces obtained after tensile testing of as-fabricated and all post-processed samples are shown in Fig. 6. Additionally, higher magnification micrographs from the center of the fracture surfaces of all the samples are shown in Fig. 7.

As can be seen in Figs. 6(a), 6(b), 6(d), and 6(f), the as-fabricated and all the samples treated at T_1=850°C undergo typical cup-cone ductile fracture. At higher magnifications, a dimpled morphology is observed due to micro-void nucleation, growth and coalescence in the center region of the fracture surfaces (Figs. 7(a), 7(b), 7(d), and 7(f)) and a shear-lip along the periphery of the fracture surfaces (Figs. 6(a), 6(b), 6(d), and 6(f)). The cup-cone fracture is, however, not evident from the fracture surfaces of the samples treated at T_1=1025°C, with or without hydrogen (Figs. 6(c), 6(e), and 6(g)). Instead, the fracture surfaces of these samples are mostly faceted (Figs. 7(c), 7(e), and 7(g)). Furthermore, the length-scale of these facets are rather comparable to the PBG size in these conditions. Nevertheless, the faceted intergranular fracture surfaces of the V1025 and 5H1025 samples are rough and contain signatures of extensive plastic deformation (Figs. 7(c) and 7(e)). However, those of 3H1025 samples are relatively smooth (Fig. 7(g)). This difference in the features of the fracture surfaces of V1025 and 5H1025 samples versus 3H1025 samples are in line with the differences in their ductility shown in Fig. 5(b).

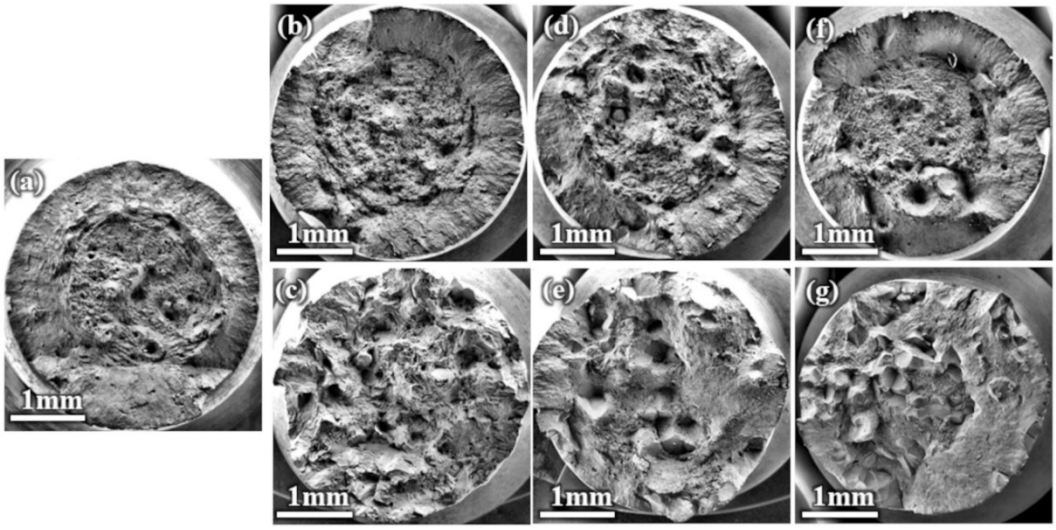

Fig. 6 – Representative SE-SEM micrographs showing the fracture surface morphology of (a) as-fabricated, (b) V850, (c) V1025, (d) 5H850, (e) 5H1025, (f) 3H850, and (g) 3H1025 samples. The scale-bar is the same for all images. A detailed description of all post-process treatments performed is given in Table I.

354

355

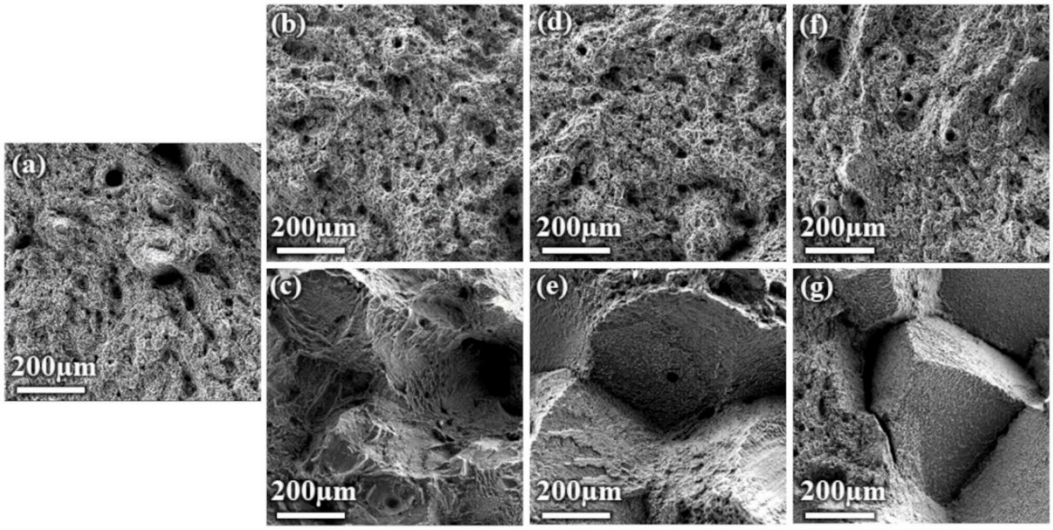

Fig. 7 – Representative high magnification SE-SEM micrographs from the center of the fracture surface of (a) as-fabricated, (b) V850, (c) V1025, (d) 5H850, (e) 5H1025, (f) 3H850, and (g) 3H1025 samples. The scale-bar is the same for all images. A detailed description of all post-process treatments performed is given in Table I.

356

IV. DISCUSSION

Herein, we explore the viability of thermohydrogen post-process treatments to achieve equiaxed PBG morphologies in EBM-processed Ti-6Al-4V without sacrificing the strength and ductility levels of the optimally-oriented, as-fabricated material. The optimal orientation that yields the best mechanical properties for the as-fabricated EBM-processed Ti-6Al-4V is commonly reported for samples tested along the build direction[12, 14]. To this end, we adapted a thermohydrogen treatment proposed by Paramore et al.[30-31]. The previous work was focused on producing Ti-6Al-4V with wrought-like mechanical properties via a powder metallurgy route and found that the best strength/ductility combinations (i.e., toughness) were obtained through a five-step thermohydrogen treatment. In the current work, we show that a three-step thermohydrogen treatment involving hydrogenation, phase transformation and dehydrogenation steps with an 850°C hydrogenation temperature (i.e., step I in Fig. I) is sufficient to transform the columnar PBGs of EBM-processed Ti-6Al-4V to equiaxed PBGs containing an ultrafine-grained α-phase morphology. Furthermore, this post-processed material had mechanical properties on par with those of the optimally-oriented as-fabricated Ti-6Al-4V samples. That is, the thermohydrogen heat-treatment improved the isotropy of the microstructure without sacrificing the mechanical properties. The maximum temperature used in the most-successful heat-treatments in this study (i.e., 850ºC) is also well below the typical β-transus temperature of hydrogen-free Ti-6Al-4V (i.e., ~990ºC[38]).

The microstructure of the EBM-processed Ti-6Al-4V contains anisotropic columnar PBGs along the build direction with a basketweave α-phase morphology within the PBGs. The transformation of these anisotropic columnar grains to isotropic equiaxed PBGs typically requires a post-process super-transus (i.e., above β-transus temperature) heat-treatment since a post-process sub-transus heat-treatment, only results in coarsening of the as-fabricated α-phase microstructure with a corresponding decrease in strength[5, 19-20]. Although a typical super-transus, post-process heat-treatment results in equiaxed PBG morphology, it also transforms the α-phase morphology from basketweave to a coarse lamellar structure which is prone to strain localization and premature fracture[20]. The coarser lamellar α-phase morphology typically found in super-transus heat-treated (i.e., β-annealed) Ti-6Al-4V results due to the preferential

nucleation of the α-phase along the PBG boundaries, which then grow into the β-grains. This results in relatively large colonies of parallel α laths with shared slip systems, allowing large slip bands to form during deformation[39]. Therefore, while typical super-transus heat-treatments address the anisotropy of EBM-processed Ti-6Al-4V, the overall mechanical performance is sacrificed.

The hydrogen introduced during the thermohydrogen treatment results in metastable β-alloy due to hydrogen's strong β-stabilizing character[40-41]. The corresponding decrease in the β-transus temperature allows engineering of the β grains from columnar to equiaxed at temperatures much lower than what is required for hydrogen-free Ti-6Al-4V. Furthermore, following hydrogenation (i.e., step I in Fig. 1) and during phase transformation (i.e., step II in Fig. 1) the material undergoes homogeneous nucleation of α_2 (Ti_3Al) and α phases, which results in orders of magnitude finer α-phase colonies than what would be produced without dissolved hydrogen present[31]. As the material continues to cool from the phase transformation heat-treatment step, it undergoes eutectoid decomposition during which a fraction of retained β-phase transforms into α and δ (TiH_2) phases.

During the dehydrogenation step (i.e., step III in Fig. 1), which involves heat-treatment at a lower temperature in a hydrogen-free atmosphere (i.e., vacuum in this study), the hydrogen is removed from the material to avoid hydrogen-induced embrittlement. The removal of hydrogen during this step also causes all the δ-phase and α_2-phase as well as some of the β-phase to transform into α-phase[30-31]. This results in an ultrafine-grained microstructure that is composed of predominantly α-phase with a small fraction of dispersed retained β-phase. Post dehydrogenation step, the material can also be subjected to globularization (i.e., step IV in Fig. 1) and aging (i.e., step V in Fig. 1)[30-32]. The globularization step is similar to a typical sub-transus heat-treatment used in the wrought processing to produce a more equiaxed microstructure, while aging is typically designed to enhance the strength of the material[39].

Our results show that post-process thermohydrogen treatments of the EBM-processed Ti-6Al-4V, at hydrogenation temperatures of 850°C or 1025°C, with or without globularization and aging, results in equiaxed PBGs with continuous grain boundary α along the PBG boundaries.

The thermohydrogen treatments with globularization and aging steps (i.e., five-step treatment) resulted in PBGs containing globularized α-phase surrounded by β-phase ribs, while treatments without globularization and ageing (i.e., three-step treatment) resulted in relatively smaller PBGs containing ultrafine-grained α-phase surrounded by dispersed retained β-phase. The effects of the hydrogenation temperature are similar in both five-step and three-step thermohydrogen treatments (i.e., increasing the hydrogenation temperature resulted in coarsening of all the microstructural features). Therefore, the thermohydrogen treatment carried out at a hydrogenation temperature of 850ºC without globularization and aging resulted in relatively smaller PBGs and finer α-phase both within the PBGs and along the PBG boundaries.

The relatively coarser microstructure of all the samples that were subjected to a five-step thermohydrogen treatment as well as five-step heat-treatment entirely in vacuum resulted in lower strength levels compared to the as-fabricated material. On the other hand, due to their relatively finer microstructure, all the samples that were subjected to a three-step thermohydrogen treatment have strength levels comparable to the as-fabricated material. Furthermore, all the samples that were subjected to a maximum post-process temperature of 850°C, irrespective of the post-process treatment atmosphere, exhibited post-necking cup-cone ductile fracture and corresponding ductility levels above or comparable to the as-fabricated material. However, all the samples that were subjected to a maximum temperature of 1025°C exhibited fracture along the PBG boundaries, thereby resulting in inferior ductility levels compared to the as-fabricated material.

V. CONCLUDING REMARKS

We have demonstrated the viability of a thermohydrogen post-process treatment to achieve equiaxed PBG morphologies in EBM-processed Ti-6Al-4V without sacrificing the mechanical properties of optimally-oriented, as-fabricated material. Specifically, our results show that a three-step thermohydrogen post-process treatment effectively transforms the columnar PBGs of EBM-processed Ti-6Al-4V into equiaxed PBGs with ultrafine α-phase. Importantly, this microstructural transformation retains the strength and ductility levels comparable to the most optimally-oriented as-fabricated samples. This three-step thermohydrogen post-process treatment

involved hydrogenation and phase transformation treatment in a hydrogen atmosphere and dehydrogenation treatment in vacuum, wherein all treatments were carried out at temperatures well below the β-transus temperature of hydrogen-free Ti-6Al-4V. Also, contrary to the previously-reported thermohydrogen-based powder metallurgy processing of Ti-6Al-4V, where adding two additional steps (globularization and ageing) resulted in further improvements in overall mechanical properties, these two additional steps for EBM-processed Ti-6Al-4V resulted in a decrease in either strength, ductility, or both. Moreover, the combination of reduced temperature requirements and the elimination of deformation-based processing substantially lowers energy costs, making this approach especially suitable for optimizing the microstructure of EBM-processed Ti-6Al-4V.

The best three-step thermohydrogen post-process treatment demonstrated herein can be further optimized. In particular, the dehydrogenation treatment in this work is carried out for 12h, which yielded residual hydrogen concentrations well below 5 ppm. This is significantly lower than the ASTM B348 standard requirement of 150 ppm for grade 5 and 125 ppm for grade 23 Ti-6Al-4V. Therefore, the processing times used herein could be reduced substantially. We hope that our results will instigate future technological development in this direction.

ACKNOWLEDGEMENTS

LDH is thankful to Michael Taylor Hurst and Daniel Oliver Lewis of Texas A&M University for their technical assistance with the hydrogenation experiments. AS gratefully acknowledges the financial support provided by the Haythornthwaite Foundation through the ASME/AMD – Haythornthwaite Research Initiation Grant and the U.S. National Science Foundation grant CMMI-1944496.

CONFLICT OF INTEREST

The authors declare that they have no conflict of interest.

REFERENCES

1. L. E. Murr, S. M. Gaytan, D. A. Ramirez, E. Martinez, J. Hernandez, K. N. Amato, P. W. Shindo, F. R. Medina and R. B. Wicker, *Journal of Materials Science & Technology,* 2012, vol. 28, pp. 1-14.
2. W. E. Frazier, *Journal of Materials Engineering and Performance,* 2014, vol. 23, pp. 1917-1928.
3. S. Liu and Y. C. Shin, *Materials & Design,* 2019, vol. 164.
4. L. Facchini, E. Magalini, P. Robotti and A. Molinari, *Rapid Prototyping Journal,* 2009, vol. 15, pp. 171-178.
5. S. S. Al-Bermani, M. L. Blackmore, W. Zhang and I. Todd, *Metallurgical and Materials Transactions A,* 2010, vol. 41, pp. 3422-3434.
6. A. A. Antonysamy, J. Meyer and P. B. Prangnell, *Materials Characterization,* 2013, vol. 84, pp. 153-168.
7. C. De Formanoir, S. Michotte, O. Rigo, L. Germain and S. Godet, *Materials Science and Engineering: A,* 2016, vol. 652, pp. 105-119.
8. Y. Kok, X. P. Tan, P. Wang, M. L. S. Nai, N. H. Loh, E. Liu and S. B. Tor, *Materials & Design,* 2018, vol. 139, pp. 565-586.
9. H. K. Rafi, N. V. Karthik, H. Gong, T. L. Starr and B. E. Stucker, *Journal of Materials Engineering and Performance,* 2013, vol. 22, pp. 3872-3883.
10. Z. Liu, B. He, T. Lyu and Y. Zou, *JOM,* 2021, vol. 73, pp. 1804-1818.
11. L. G. and W. J. C.: *Titanium*. Second ed. (Springer Science & Business Media, 2007).
12. P. Nandwana, Y. Lee, C. Ranger, A. D. Rollett, R. R. Dehoff and S. S. Babu, *Metallurgical and Materials Transactions A,* 2019, vol. 50, pp. 3429-3439.
13. M. Fang, F. Hu, Y. Han, J. Le, J. Xi, J. Song, L. Ke, M. Xiao and W. Lu, *Materials Science and Engineering: A,* 2021, vol. 827, p. 142031.
14. M. Seifi, A. Salem, D. Satko, J. Shaffer and J. J. Lewandowski, *International Journal of Fatigue,* 2017, vol. 94, pp. 263-287.
15. H. Gong, K. Rafi, H. Gu, G. D. Janaki Ram, T. Starr and B. Stucker, *Materials & Design,* 2015, vol. 86, pp. 545-554.
16. T. Montalbano, B. N. Briggs, J. L. Waterman, S. Nimer, C. Peitsch, J. Sopcisak, D. Trigg and S. Storck, *Journal of Materials Processing Technology,* 2021, vol. 294, p. 117113.
17. S. P. Narra, A. D. Rollett, A. Ngo, D. Scannapieco, M. Shahabi, T. Reddy, J. Pauza, H. Taylor, C. Gobert and E. Diewald, *Journal of Materials Processing Technology,* 2022, p. 117775.
18. R. Cunningham, A. Nicolas, J. Madsen, E. Fodran, E. Anagnostou, M. D. Sangid and A. D. Rollett, *Materials Research Letters,* 2017, vol. 5, pp. 516-525.
19. H. Galarraga, R. J. Warren, D. A. Lados, R. R. Dehoff, M. M. Kirka and P. Nandwana, *Materials Science and Engineering: A,* 2017, vol. 685, pp. 417-428.
20. L. Draelos, P. Nandwana and A. Srivastava, *Materials Science and Engineering: A,* 2020, p. 139986.
21. Y. Zhou, K. Wang, Z. Sun and R. Xin, *Journal of Materials Processing Technology,* 2022, vol. 306, p. 117607.
22. J. Liu, G. Li, Q. Sun, H. Li, J. Sun and X. Wang, *Journal of Materials Processing Technology,* 2022, vol. 299, p. 117366.

23. M. Jamshidinia, M. M. Atabaki, M. Zahiri, S. Kelly, A. Sadek and R. Kovacevic, *Journal of Materials Processing Technology,* 2015, vol. 226, pp. 264-271.
24. M. J. Bermingham, D. Kent, H. Zhan, D. H. Stjohn and M. S. Dargusch, *Acta Materialia,* 2015, vol. 91, pp. 289-303.
25. O. N. Senkov and F. H. Froes, *International Journal of Hydrogen Energy,* 1999, vol. 24, pp. 565-576.
26. D. H. Kohn and P. Ducheyne, *Journal of Materials Science,* 1991, vol. 26, pp. 328-334.
27. M. Niinomi, B. Gong, T. Kobayashi, Y. Ohyabu and O. Toriyama, *Metallurgical and Materials Transactions A,* 1995, vol. 26, pp. 1141-1151.
28. F. H. Froes, O. N. Senkov and J. I. Qazi, *International Materials Reviews,* 2004, vol. 49, pp. 227-245.
29. Z. Sun, W. Zhou and H. Hou, *International Journal of Hydrogen Energy,* 2009, vol. 34, pp. 1971-1976.
30. J. D. Paramore, Z. Z. Fang, P. Sun, M. Koopman, K. S. R. Chandran and M. Dunstan, *Scripta Materialia,* 2015, vol. 107, pp. 103-106.
31. J. D. Paramore, Z. Z. Fang, M. Dunstan, P. Sun and B. G. Butler, *Sci Rep,* 2017, vol. 7, p. 41444.
32. M. Knezevic, S. Ghorbanpour, N. C. Ferreri, I. A. Riyad, A. D. Kudzal, J. D. Paramore, S. C. Vogel and B. A. Mcwilliams, *Materials Science and Engineering: A,* 2021, vol. 809, p. 140980.
33. H. Galarraga, D. A. Lados, R. R. Dehoff, M. M. Kirka and P. Nandwana, *Additive Manufacturing,* 2016, vol. 10, pp. 47-57.
34. *ASTM E1447-09: Standard Test Method for Determination of Hydrogen in Titanium and Titanium Alloys by Inert Gas Fusion Thermal Conductivity/Infrared Detection Method* (ASTM International
2016).
35. *ASTM E8/E8M-21: Standard Test Methods for Tension Testing of Metallic Materials* (ASTM International, 2021).
36. *ASTM B348-10: Standard Specification for Titanium and Titanium Alloy Bars and Billets* (ASTM International, 2010).
37. *ASTM E112-13: Standard Test Methods for Determining Average Grain Size* (ASTM International, 2021).
38. G. C. Obasi, S. Birosca, J. Q. Da Fonseca and M. Preuss, *Acta Materialia,* 2012, vol. 60, pp. 1048-1058.
39. L. G. and W. J.C.: *Titanium*. Second ed. (Springer Science & Business Media, 2007).
40. P. Sun, Z. Z. Fang, M. Koopman, J. Paramore, K. R. Chandran, Y. Ren and J. Lu, *Acta Materialia,* 2015, vol. 84, pp. 29-41.
41. P. Sun, Z. Z. Fang, M. Koopman, Y. Xia, J. Paramore, K. Ravi Chandran, Y. Ren and J. Lu, *Metallurgical and Materials Transactions A,* 2015, vol. 46, pp. 5546-5560.